NeuroImage 196 (2019) 200–206

Contents lists available at ScienceDirect

NeuroImage

journal homepage: www.elsevier.com/locate/neuroimage

Structural mapping with fiber tractography of the human cuneate fasciculus at microscopic resolution in cervical region

Ahmet Fatih Atik [a,*], Evan Calabrese [c], Robert Gramer [a], Syed M. Adil [a], Shervin Rahimpour [a], Promila Pagadala [a], G. Allan Johnson [b], Shivanand P. Lad [a]

[a] Department of Neurosurgery, Duke University Medical Center, Durham, NC, USA
[b] Department of Biomedical Engineering, Duke University, Durham, NC, USA
[c] Department of Radiology and Biomedical Imaging, University of California San Francisco, San Francisco, CA, USA

A B S T R A C T

Human spinal white matter tract anatomy has been mapped using post mortem histological information with the help of molecular tracing studies in animal models. This study used 7 Tesla diffusion MR tractography on a human cadaver that was harvested 24 hours post mortem to evaluate cuneate fasciculus anatomy in cervical spinal cord. Based on this method, for the first time much more nuanced tractographic anatomy was used to investigate possible new routes for cuneate fasciculus in the posterior and lateral funiculus. Additionally, current molecular tracing studies were reviewed, and confirmatory data was presented along with our radiological results. Both studies confirm that upon entry to the spinal cord, upper cervical level tracts (C1-2-3) travel inside lateral funiculus and lower level tracts travel medially inside the posterior funiculus after entry at posterolateral sulcus which is different than traditional knowledge of having cuneate fasciculus tracts concentrated in the lateral part of posterior funiculus.

1. Introduction

Spinal cord anatomy has been a topic of study for nearly 2 millennia, dating back to Galen's second-century work describing a spinal cord enveloped by dural and pial coverings encased by vertebrae unified by a posterior longitudinal ligament. A long hiatus followed, however, until Avicenna's eleventh-century research described spinal cord in detail and as continiuum of the brain to carry motor nerves and myelin sheet as a protective fatty layer over the nerves (Mazengenya and Bhikha, 2017; Naderi et al., 1449). Furthermore, his description of anterior and posterior roots provided the groundwork for the eighteenth-century experiments of Mistichelli and Pourfoir du Petit which revealed the pyramidal decussation and the presence of discrete tracts within the cord's structure followed by Huber's identification of the ordered spinal roots and denticulate ligaments (Mazengenya and Bhikha, 2017; Naderi et al., 2004). While significant, the understanding of spinal cord anatomy up unto this time had relied exclusively upon gross anatomical observation. Stilling's invention of the microtome and advent of frozen histological sectioning afforded a novel cross-sectional, microscopic view of the cord, catapulting the understanding of spinal cord anatomy forward during the nineteenth century. During this time, the extensive work of Brown-Sequard elucidated sensory tract decussation, and various transection and lesioning experiments by Burdach, Turck, Clarke, Lissauer, Goll, Flechsig, Gowers, Bastian, and Flatau demonstrated how motor, sensory, and reflex functions were affected by local disruption along the cord, and therein, where tracks reside throughout the cord (Naderi et al., 2004).

The introduction of electrophysiology and the innovation of various imaging modalities, namely magnetic resonance, have helped to enrich these discoveries over the past century; however, the understanding of human spinal cord architecture remains largely incomplete, residing at the tract level, with very little insight into how fibers organize within and between the various columns. While the conceptualization of the spinal cord as a bundle of modality-specific tracts is invaluable in localizing function, or lack thereof, work in neuroregeneration, neurorehabilitation, neurodevelopment, and neuromodulation stand to benefit from a better understanding of not just how these tracts are organized relative to each other, but moreover, how these tracts are organized in and of themselves.

Most of the current literature on spinal white matter pathways was produced with the assistance of molecular tracing studies in the late 1980s and early 1990s (Apkarian and Hodge, 1989)' (Davidoff, 1990)' (Nathan et al., 1996). Recently, there has been an augmented interest in this area of research (Hilton et al., 2013; Liao et al., 2015); however, most of the current textbooks still apply and reference the work from the 1990s. The posterior column conveys sensations of proprioception,

* Corresponding author. Department of Neurosurgery, Duke University Medical Center, Box 3807, Durham, NC, 27710, USA.
E-mail address: ahmetfatihatik@gmail.com (A.F. Atik).

https://doi.org/10.1016/j.neuroimage.2019.04.030
Received 25 September 2018; Received in revised form 4 February 2019; Accepted 8 April 2019
Available online 11 April 2019

vibration, two-point discrimination, and fine touch via two distinct white matter tracts: the gracile fasciculus, which conveys lower extremity afferent fibers, and the cuneate fasciculus, which conveys the upper extremity afferent fibers. These fiber tracts ascend to the level of the medulla oblongata where they synapse in the ipsilateral cuneate nucleus and gracile nucleus, respectively, before decussating and projecting to the contralateral thalamus via the medial lemniscus.

In this study, the organization of the cuneate fascicule in the cervical spinal cord was investigated. Our research also examined the possibility of new cuneate fasciculus routes in the posterior column. Current data suggests that rootlets enter the spinal cord through the posterior lateral sulcus and ascend inside Lissauer's lamina before entering the posterior column and converging in the lateral posterior funiculus in the cuneate fasciculus. Our study uses a high-resolution diffusion MRI tractography method to investigate these tracts in a human spinal cord that was excised and fixed within 24 h postmortem. We also review current literature for confirmatory molecular tracing studies to validate our results.

This analysis builds upon our prior publication of magnetic resonance microscopy (MRM) of the human spinal cord. This approach provides 50um isotropic resolution anatomic image data and 100um isotropic resolution diffusion data, made possible by a 280 h long multi-segment acquisition and automated image segment composition. For the first time, this allows a much more nuanced understanding of spinal cord structures, such as the cuneate fasciculus, and can potentially improve conservation of its function during intramedullary tumor resection, restoration of its connections following injury, targeting ablation techniques such as dorsal root entry zone (DREZ) lesioning, and modulation of pain through focused spinal cord and dorsal root ganglion stimulation. More generally, better localization of white matter tracts, as well as fiber trajectory within specific tracts, can help guide future tailored surgical, regenerative, and modulatory measures throughout the spinal cord. Our findings reveal that the intraspinal organization of the cuneate fasciculus in the posterior funiculus challenges traditional knowledge and we propose the possibility of a new high-resolution radiological map for dorsal cervical tract fibers by using a novel MRM tracking technique.

2. Material and methods

2.1. Specimen procurement

An entire human spinal cord (pyramidal decussation to cauda equina) was obtained from a deceased adult male with no known history of neurologic disease. After the death and prior to spinal cord removal, the cadaver was gravity perfused with normal saline through the right carotid artery until all visible blood was flushed from the vascular system. The time between death and organ harvest (postmortem interval) was approximately 18 hours and during this time the cadaver was maintained at 4 °C. Spinal cord extraction was performed by a trained neurosurgeon using standard surgical instruments.

2.2. Specimen preparation

Immediately after extraction, the dura was opened longitudinally, and the spinal cord was sutured via the attached dural flaps to a block of closed-cell polystyrene foam in a fully extended position. This step was done to ensure that the cord remained straight and suspended during subsequent fixation. The specimen was immersion fixed in a 10% formalin solution for 1 week. The specimen was then transferred to a phosphate buffered saline solution with 2.5 mM gadoteridol for 1 week prior to scanning. Immediately prior to scanning, the spinal cord was completely dissected away from the dura, placed in a custom-machined plastic specimen tube, and immersed in Galden HT-200 liquid fluorocarbon (Solvay, Brussels, Belgium) for magnetic susceptibility matching and to prevent specimen dehydration during scanning.

2.3. Imaging hardware

MR imaging was performed on 7T horizontal-bore small animal MRI system (Magnex Scientific, Yarton, Oxford, UK), controlled by an Agilent console running VnmrJ 4.0 (Agilent Technologies, Santa Clara, CA, USA). Radiofrequency transmission and reception were accomplished with a custom-made cylindrical quadrature coil measuring 11 cm long with a 3.1 cm inner diameter. The coil was affixed to a custom fabricated magnet gantry insert with a 100 cm long sliding inner specimen tube featuring locking distance marks at 1 cm intervals. This device was designed to allow precise specimen movements in the magnet Z-axis (along with the bore) without allowing rotation or translation in other axes.

2.4. Image acquisition

MR images of the entire cord were acquired in 7 separate overlapping segments (segment FOV 8 × 2 × 2 cm with 1 cm of overlap on each end). Between each acquisition, the specimen was advanced precisely 7 cm through the magnet bore using the previously described gantry insert. T2*-weighted anatomic images were acquired using a 3D gradient echo sequence with an acquisition matrix of 1600 × 400 x 400, resulting in 50-μm isotropic resolution. Diffusion-weighted images were acquired using a simple diffusion-weighted spin echo sequence with an acquisition matrix of 800 × 200 x 200, resulting in 100-μm isotropic resolution. A total of 30 non-collinear diffusion-weighted images ($b = 4000$ s/mm^2) and 3 $b = 0$ s/mm^2 images were acquired. Total acquisition time was approximately 280 h.

The use of formalin fixed tissue, while necessary for the high spatial resolution diffusion imaging that this work is based on, has several important limitations. Formalin fixation is known to induce an approximately 4-fold decrease in tissue diffusivity. This effect can be partially compensated for by using 4-fold higher diffusion weighting (i.e. b-values) (Dyrby et al., 2011). For this study, we used $b = 4000$ s/mm^2, which corresponds to approximately $b = 1000$ s/mm^2 for in-vivo tissue. Unfortunately, the structural changes induced by formalin fixation may not be entirely isotropic. For example, a previous diffusion MRI study of ex-vivo cervical spinal cord segments found that tissue fixation disproportionally reduced longitudinal diffusivity, but not radial diffusivity or anisotropy (Kim et al., 2009).

2.5. Image processing

Images were reconstructed, gradient unwarped, and digitally combined using a custom-developed image processing pipeline implemented in MATLAB (MathWorks, Natick, MA, USA). Gradient unwarping code was adapted from the General Electric Gradwarp gradient nonlinearity correction tool (GE, Boston, MA, USA). Image segments were combined into a single image by automated image registration of overlapping ends (ANTs, http://picsl.upenn.edu/software/ants/) and subsequent weighted averaging. The final composite FOV was 47 × 2 × 2 cm. Diffusion data processing and tractography were performed in DSI studio (http://dsi-studio.labsolver.org/). The fiber reconstruction algorithm was Generalized Q-Sampling Imaging (GQI), using default parameters (Yeh et al., 2010).

2.6. Fiber tracking

The first step of creating a tractography route for an individual spinal cord root is to select the appropriate seeding area. To better serve the purpose of this study, dorsal roots were defined on the DSI studio software and seeding areas were selected using the lasso tool on the software. This allowed us to draw borders around the root. Based on our experience, the maximum number of fibers can be achieved by choosing the seeding area immediately proximal to the dorsal root ganglion. Each seeding area was drawn on axial, sagittal and coronal planes, (Fig. 1).

Also one Region of Interest (ROI) was drawn at C1 level that covers lateral and posterior columns to encompass all possible areas that cervical dorsal tracts might pass. Tracking parameters included a tracking FA threshold $\leq$0.02, an angular threshold $\leq$45° for the tracts that carry sensory information and $\leq$60° for tracts that decussate inside the spinal cord, a maximum tract length of 450 mm (average length of human spinal cord), trilinear tract interpolation, and deterministic tracking. Of note, deterministic tractography has a tendency to occasionally create obviously erroneous tracking patterns (i.e. an immediately terminal cuneate to pyramidal projection). As such, we selected regions of avoidance to mitigate these tracking errors.

3. Results

Our laboratory describes a novel tracking strategy by choosing ROIs proximal to the dorsal root ganglion and create a tracking strategy up towards the C1 level, hence we have called it Root Back-Tracking Method (RBTM). We have been able to gather tangible and reliable data using this approach and the results have been much better than selecting an ROI in higher cervical sections.

Dorsal roots enter the spinal cord from the posterolateral sulcus (Fig. 2A). Upon entering, tracts ascend in Lissauer's tract shortly and then move into posterior funiculus, C5 has been shown as an example in Fig. 2B.

As the tracts ascend inside the posterior fasciculus, they also move medially, this can be appreciated by looking at the location of entry and location of same tract group above C5. Fig. 3A represents C5 fiber tracts at the C4 level, and 3B, 3C, 3D show tract distribution at levels C3, C2 and C1 respectively. This pattern can be seen with other sensorial cervical tracts as well. As the distance becomes longer, tracts tend to move more medially, hence C8 tracts are located in a most medial location away from the posterior edge of spinal cord and closer to gray matter.

Fig. 4A depicts all 8 cervical dorsal tracts that travel inside the posterior column. The C1 fibers are mostly confined to Lissauer's tract (C1-dark blue). The C2 fibers are located in Lissauer's tract as well as the lateral funiculus (C2-light blue). C3 and C4 comprise fewer number of fibers, most of which are located in either Lissauer's (C3-Beige color) or in the lateral part of cuneate fasciculus (C4-yellow). C5 is in the same color as in Fig. 3(C5-orange) andis in the posteromedial part of cuneate fasciculus border. Note that only the C3, C4 and part of C5 are in the previously described cuneate fasciculus area. Moving caudally, the fibers of C6 (dark pink), C7 (light pink), and C8(red) are concentrated in the medial part of right half of posterior funiculus, in the area that is previously described as gracile fasciculus.

4. Discussion

This analysis builds upon our prior publication of magnetic resonance microscopy (MRM) of the human spinal cord (Calabrese et al., 2018). This approach provides 50um isotropic resolution anatomic image data and 100um isotropic resolution diffusion data. For the first time, this allows a much more nuanced understanding of spinal cord structures, such as the cuneate fasciculus, and the present study demonstrates that the distribution of the cervical dorsal sensory fibers constitutes a much larger area than previously described, expanding outside of the cuneate fasciculus to include portions of the traditionally demarcated gracile fasciculus in the lateral funiculus.

As cited in Fig. 5, our findings corroborate a recent molecular tracing study that challenges the established framework of the distributions of cervical dorsal sensory fibers. In a molecular tracing study detailing the anatomical cuneate fasciculus, Liao et al. demonstrated that the distribution of the cuneate fibers incorporates into the lateral funiculus, Lissauer's tract, lateral posterior funiculus and medial posterior funiculus (Liao et al., 2015). Performing molecular tracing methods on live humans is technically and ethically challenging, therefore utilization of MRM of the human spinal cord is a valuable method to better understand human spinal cord white matter anatomy. Moreover, the fibers that come from lower cervical levels (C5, C6, C7, C8) travel along the posterior border of the spinal cord and encompass the medial part of spinal hemisection in posterior funiculus. Conversely, while our studies describe a more expanded distribution, previous tractography studies by De Leener et al., Fitzgibbons et al., and Soria et al. (De Leener et al., 2017; Fitzgibbons, 2016; Soria et al., 2011) all demonstrate a more localized distribution of the sensory fibers to only the lateral part of posterior funiculus (see Fig. 6).

Clinical translation of this data can be applied in a number of ways. Neuromodulation approaches, such as Spinal Cord Stimulation (SCS), are a commonly performed technique for treating intractable neuropathic

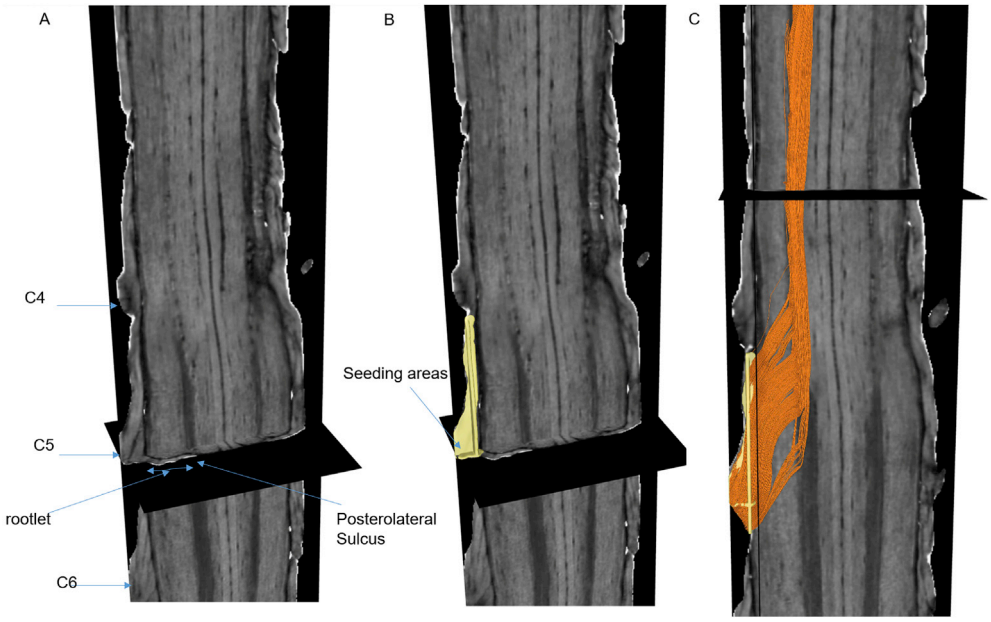

Fig. 1. Spinal Cord from posterior coronal view. A) Left dorsal roots are shown at the level of C4—C5 and C6. rootlets enter the spinal cord at posterolateral sulcus(shown) B) Seeding areas of the C5 root, proximal to dorsal root ganglion before entering the spinal cord. C) Post tracking, only C5 fibers are shown. 4 rootlets are entering to spinal cord separately at posterolateral sulcus.

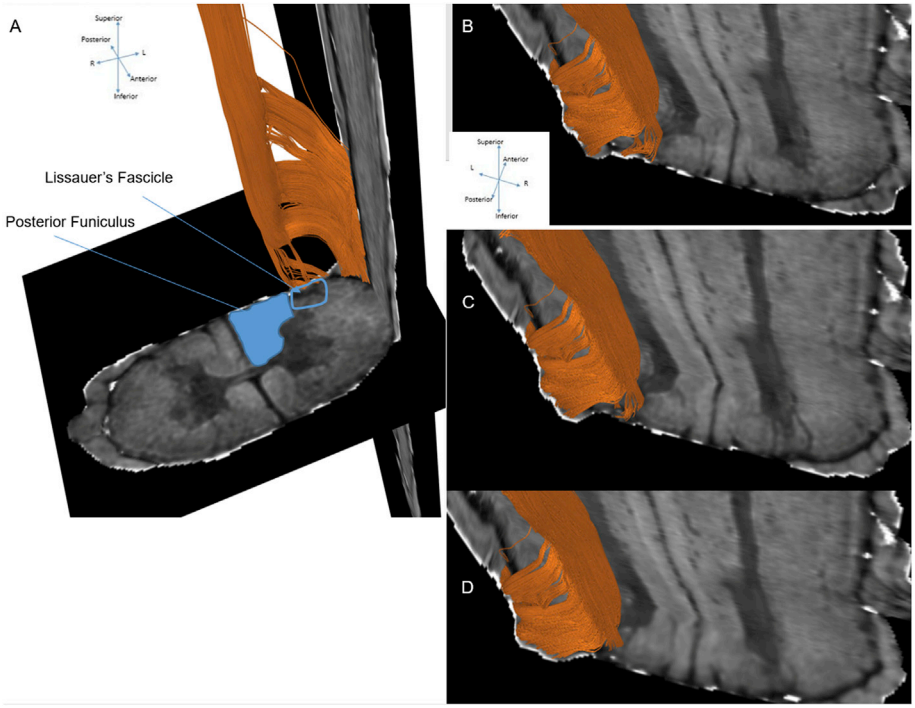

Fig. 2. Entry of left dorsal C5 rootto the spinal cord. A) Coronal section from anterior-superior angle. Complete area of lateral half of posterior funiculus is painted in blue. Circled area depicts Lissauer's fascicle as an entry point for C5 dorsal rootlets. B) Coronal section from posterior-superior angle shows the entry of most inferior C5 rootlet to Lissauer's fascicle and ascension inside the spinal cord. C) C5 Tract ascends inside the Lissauer's tract D) C5 tract moves into posterior funiculus. Subsequently rest of the C5 rootlets will follow the same path and converge in posterior funiculus.

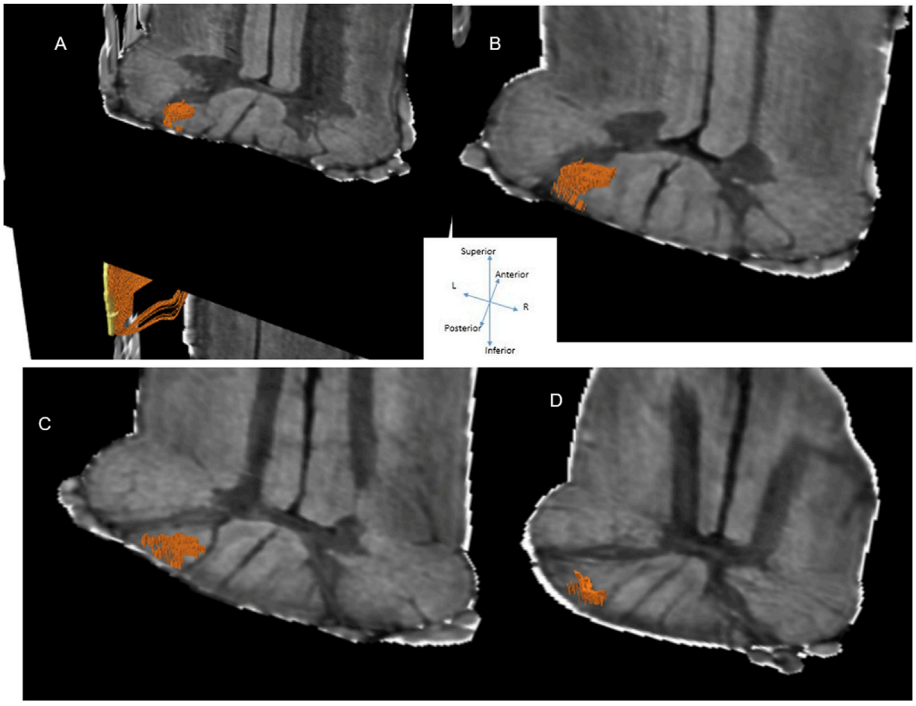

Fig. 3. Coronal section of the spinal cord from a posterior-superior angle. A) Entry of C5 sensory root to Lissauer's fascicle from dorsolateral sulcus at C4 level. B) Axial plane is moved to C3 level. C5 fibers are grouped in the lateral portion of posterior funiculus C) Axial plane at the C2 level, C5 fibers are moving medially. D) The axial plane at the C1 level and C5 fibers at their most medial location.

pain. Currently, electrodes are being placed several levels above the corresponding dermatomes of a patient's painful region. Furthermore, many times, the leads are simply placed in the upper cervical spine and a variety of contact configurations are relied upon to stimulate the desired spinal cord structures corresponding to the patient's symptoms. For a patient who has a bilateral arm, shoulder or neck pain, SCS leads are placed along the midline cervical epidural space. Contacts at the tip of electrodes can be marked as anode or cathode and electrical stimulation is achieved and finally, pain reduction is achieved after optimization process with different settings. Typical maximum depth of current from SCS is 1–2 mm inside the dorsal aspect of the spinal cord, with a variety of potential structures in the vicinity including dorsal column, dorsal roots and the dorsal root entry zone (Holsheimer, 2002). Understanding the distribution of afferent fibers in the dorsal column might allow clinicians

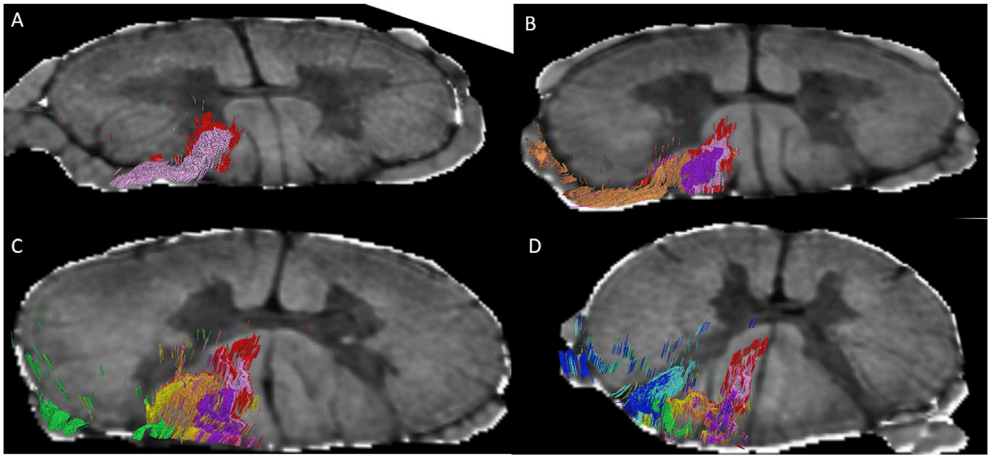

Fig. 4. Comparison of axial section of Cervical tractography for Cuneate fascicle. A) A cut-section at C7 shows somatotopy of C7 and C8 tracts located mostly in lateral part of posterior column. B) Cut section at C5 shows C5-6-7 and C8 tracts moving medially. C) Cut-section at C3 shows C3-4-5-6 and C8 tracts started to move in the area previously known as Gracile fascicle area. D) Cut-section at C1 shows all cervical dorsal tracts that belongs to Cuneate fascicle. Lower cervical tracts located inside previously known Graciel fascicle. Color code: C1 dark blue, C2 light blue, C3 green, C4 yellow, C5 orange, C6 purple, C7 light pink, C8 red.

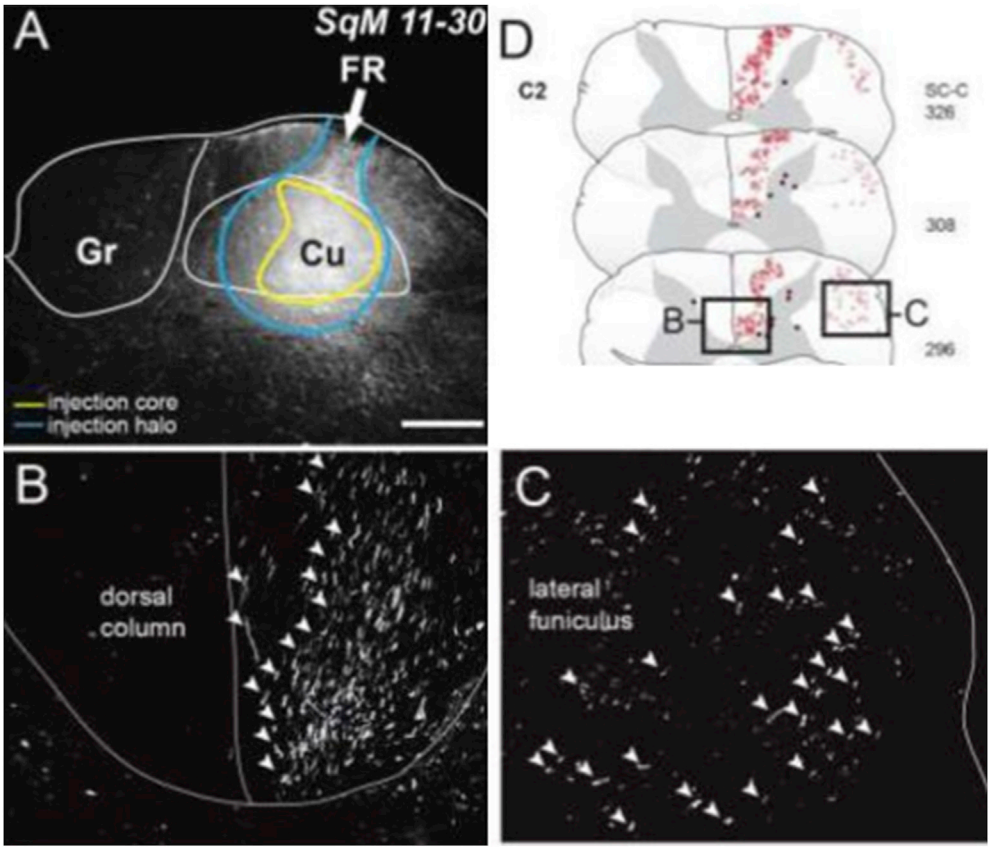

Fig. 5. Data courtesy of Kaas lab, Vanderbilt University (PMID: 25845707). Locations of axons connecting the cuneate nucleus and cervical spinal cord labeled by injection of fluoro-ruby (FR) into the cuneate nucleus of squirrel monkey 11–30. A) The FR injection site is confined to the cuneate nucleus. B) A great number of FR-labeled fibers are located across the depth of the cuneate fasciculus (box in D). The labeled-fibers are marked by arrowheads. This section is at C2 therefore tracts have not yet moved to most medial part of posterior column but they match to distribution in our data. C) A small number of FR-labeled fibers are in the dorsal portion of the lateral funiculus (box in D). D) The distributions of FR-labeled fibers (red) are mainly in the dorsal column and fewer of them are in the lateral funiculus. The densities of labeled fibers are reduced to caudal segments from C2 to C5. The FR-labeled neurons are mainly distributed in the dorsal horn of the cervical spinal cord ipsilateral to the injection site, and few of the labeled neurons are located on the contralateral side. Scale bar is 0.5 mm in A and 250 μm in B – C (Liao et al., 2015).

the opportunity to better address symptoms and place the leads accordingly. Because upper cervical sensory tracts are located more laterally and lower cervical sensory tracts more centrally, lead positioning and programming strategies might be reconsidered according to the patient's specific anatomy and pain symptoms.

Describing a seed area for any intraspinal tract can be challenging, due to the existence of numerous ascending and descending tracts in the cervical spinal cord. Also, as we showed in this study, the location of an individual group of tracts using high resolution techniques such as MRM, may be different when compared to classical knowledge. To surround all necessary tracts in the posterior funiculus each root is selected as a seed area and tracking is started after defining the termination point immediately above C1 level, which is also the upper limit of our specimen. To our knowledge, this Root Back-Tracking Method (RBTM) of incorporating the dorsal roots as the seeding area has not been reported in the literature. Classical tractography method was described by Conturo et al. and Catani et al., in 1999 and 2002 respectively (Catani et al., 2002; Conturo et al., 1999). These researchers used their methods only in cerebral tissue and it's been working properly for intracranial tractography studies for more than a decade. RBTM is designed for spinal tractography where intramedullary areas contain extremely dense tractography data. Using the methods previously described came up with unreliable and less then optimal data therefore we used most well-defined areas (roots) as seeding areas with axial and sagittal ROIs.

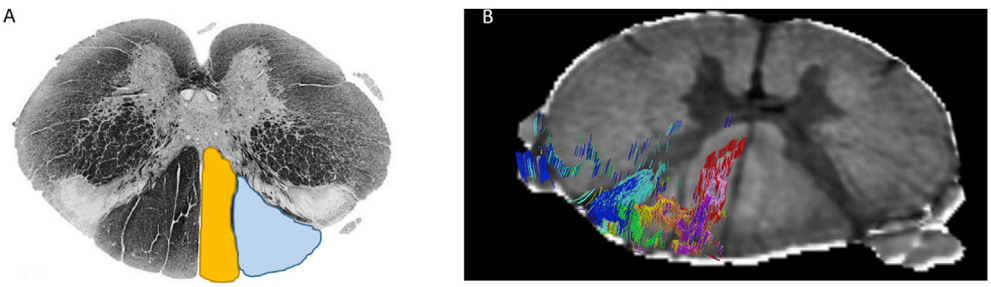

Fig. 6. Comparison of two cut-section images at C1. A) Anatomy of human spinal cord axial view. Right posterior column is divided into two parts, the lateral (light blue) part is known to be cuneate fasciculus and the medial (yellow) part is Gracile fasciculus. B) Our tractographic findings demonstrate wider distribution of cuneate fasciculus in the left posterior column. Lower cervical tracts appear to be located more medially. Color code: C1 dark blue, C2 light blue, C3 beige, C4 yellow, C5 orange, C6 purple, C7 light pink, C8 red.

Also using another ROI at C1 level covering posterior and lateral columns increased our tract quality significantly. It is fair to say that this method is modification of previous methods and application to a new area. The success of this method lies in perhaps because previous studies have lacked the spatial resolution necessary to back-track rootlets in the human spinal cord.

Previous Diffusion MRI Tractography studies in the human spinal cord have heavily focused upon preoperative planning (Choi et al., 2014), evaluating the effect of specific surgeries (Lee et al., 2013) and change in anisotropy and diffusivity after correction of certain pathologies such as Chiari Malformation (CM) (Merlini et al., 2012) or space-occupying lesions (Takano et al., 2013). To our knowledge, this research is the first fiber tractography data using MRM's high-resolution 100um diffusion MRI spinal cord images to define individual routes for cervical roots in the cuneate fasciculus. Previous studies lacked in resolution and because tracking methods used intramedullary ROIs or whole spine, therefore provided less specificity (Brander et al., 2014; Egger et al., 2016; Zhao et al., 2017). While molecular tracing studies would serve as a gold standard for outlining these tracts, such a measure is currently not feasible in live humans. MRM provides insight into the intricacies of the human spinal cord white matter anatomy that cannot otherwise be appreciated by alternative means. The use of software to track fibers introduces the potential for false positive and negative results; however, relative to probabilistic tractography, deterministic tractography in conjunction with prudent regional restriction and a high-resolution image data set minimizes this potential.

Diffusion tractography is both a commonly used and powerful technique for exploring axonal connections in the central nervous system, however there are fundamental limitations to the types of connections that can be modeled (Calabrese et al., 2015; Thomas et al., 2014)For example, diffusion tractography is limited in its ability to represent intravoxel fiber crossing and is incapable of representing other complex intravoxel fiber geometries such as “kissing” or “fanning” fibers. Further, even at the microscopic image resolution presented in this work, diffusion-based tracts represent averages of hundreds to thousands of individual axons. Finally, tractography does not provide any insight into neuronal synapses or the direction of information flow within a tract.

Our findings on the somatotopic organization of cervical cuneate corresponds with a recent molecular tracing study that was executed by Kaas Lab at Vanderbilt University (Liao et al., 2015). The authors injected retrograde tracer fluoro-ruby(FR) to the cuneate nucleus of squirrel monkey and traced through white matter in the spine. Their findings show similar distribution pattern with our radiological distribution. Lower cervical cuneate fasciculus tracts are more medial and upper levels mostly on lateral to the posterior column and in lateral funiculus (Fig. 5).

5. Conclusion

In conclusion, cervical dorsal sensory fiber tracts appear to be distributed across the traditional lateral funiculus to the median sulcus in the posterior funiculus, a much larger area compared to previously believed confines of the cuneate fasciculus. We corroborate these results with the latest molecular tracing data. Tractography via a high-field scanner of an externalized human spinal cord provides a unique opportunity to study the fiber architecture of the long-appreciated, but poorly understood tracts of the human spinal cord. More studies are needed to confirm and build upon our results. The field of magnetic resonance microscopy (MRM) is still in its infancy, but it allows a much more nuanced understanding of spinal cord structures than ever before.

Appendix A. Supplementary data

Supplementary data to this article can be found online at https://doi.org/10.1016/j.neuroimage.2019.04.030.

Funding

National Center for Advancing Translational Sciences of the National Institutes of Health, Award Number UL1TR001117. National Institute of Health/ National institute of Biomedical Imaging and Bioengineering (NIH/NIBIB), National Biomedical Technology Resource Center (P41 EB015897 to GA Johnson), NIH 1S10OD010683-01 (to GA Johnson).

References

Apkarian, A.V., Hodge, C.J., 1989. Primate spinothalamic pathways: II. The cells of origin of the dorsolateral and ventral spinothalamic pathways. J. Comp. Neurol. 288, 474–492.
Brander, A., Koskinen, E., Luoto, T.M., Hakulinen, U., Helminen, M., Savilahti, S., et al., 2014. Diffusion tensor imaging of the cervical spinal cord in healthy adult population: normative values and measurement reproducibility at 3T MRI. Acta Radiol. 55, 478–485.
Calabrese, E., Adil, S.M., Cofer, G., Perone, C.S., Cohen-Adad, J., Lad, S.P., et al., 2018. Postmortem diffusion MRI of the entire human spinal cord at microscopic resolution. Neuroimage Clin 18, 963–971.
Calabrese, E., Badea, A., Cofer, G., Qi, Y., Johnson, G.A., 2015. A diffusion MRI tractography connectome of the mouse brain and Comparison with neuronal tracer data. Cerebr. Cortex 25, 4628–4637.
Catani, M., Howard, R.J., Pajevic, S., Jones, D.K., 2002. Virtual in vivo interactive dissection of white matter fasciculi in the human brain. Neuroimage 17, 77–94.
Choi, K.S., Kim, M.S., Kwon, H.G., Jang, S.H., Kim, O.L., 2014. Preoperative identification of facial nerve in vestibular schwannomas surgery using diffusion tensor tractography. J Korean Neurosurg Soc 56, 11–15.
Conturo, T.E., Lori, N.F., Cull, T.S., Akbudak, E., Snyder, A.Z., Shimony, J.S., et al., 1999. Tracking neuronal fiber pathways in the living human brain. Proc. Natl. Acad. Sci. U. S. A. 96, 10422–10427.
Davidoff, R.A., 1990. The pyramidal tract. Neurology 40, 332–339.
De Leener, B., Levy, S., Dupont, S.M., Fonov, V.S., Stikov, N., Louis Collins, D., et al., 2017. SCT: spinal Cord Toolbox, an open-source software for processing spinal cord MRI data. Neuroimage 145, 24–43.
Dyrby, T.B., Baare, W.F., Alexander, D.C., Jelsing, J., Garde, E., Sogaard, L.V., 2011. An ex vivo imaging pipeline for producing high-quality and high-resolution diffusion-weighted imaging datasets. Hum. Brain Mapp. 32, 544–563.
Egger, K., Hohenhaus, M., Van Velthoven, V., Heil, S., Urbach, H., 2016. Spinal diffusion tensor tractography for differentiation of intramedullary tumor-suspected lesions. Eur. J. Radiol. 85, 2275–2280.
Fitzgibbons, M.S.N., 2016. Primer of brainstem anatomy: a detailed examination of anatomy and pathology through MRI and DTI. Neurographics 6, 76–87.
Hilton, B.J., Assinck, P., Duncan, G.J., Lu, D., Lo, S., Tetzlaff, W., 2013. Dorsolateral funiculus lesioning of the mouse cervical spinal cord at C4 but not at C6 results in sustained forelimb motor deficits. J. Neurotrauma 30, 1070–1083.
Holsheimer, J., 2002. Which neuronal elements are activated directly by spinal cord stimulation. Neuromodulation 5, 25–31.

Kim, T.H., Zollinger, L., Shi, X.F., Rose, J., Jeong, E.K., 2009. Diffusion tensor imaging of ex vivo cervical spinal cord specimens: the immediate and long-term effects of fixation on diffusivity. Anat. Rec. 292, 234–241.

Lee, M.J., Kim, H.D., Lee, J.S., Kim, D.S., Lee, S.K., 2013. Usefulness of diffusion tensor tractography in pediatric epilepsy surgery. Yonsei Med. J. 54, 21–27.

Liao, C.C., DiCarlo, G.E., Gharbawie, O.A., Qi, H.X., Kaas, J.H., 2015. Spinal cord neuron inputs to the cuneate nucleus that partially survive dorsal column lesions: a pathway that could contribute to recovery after spinal cord injury. J. Comp. Neurol. 523, 2138–2160.

Mazengenya, P., Bhikha, R., 2017. The structure and function of the central nervous system and sense organs in the canon of medicine by Avicenna. Arch. Iran. Med. 20, 67–70.

Merlini, L., Fluss, J., Korff, C., Hanquinet, S., 2012. Partial rhombencephalosynapsis and Chiari type II malformation in a child: a true association supported by DTI tractography. Cerebellum 11, 227–232.

Naderi S, Acar F, Mertol T, Arda MN: Functional anatomy of the spine by Avicenna in his eleventh century treatise Al-Qanun fi al-Tibb (The Canons of Medicine). Neurosurgery 52:1449-1453; discussion 1453-1444, 2003

Naderi, S., Ture, U., Pait, T.G., 2004. History of the spinal cord localization. Neurosurg. Focus 16, E15.

Nathan, P.W., Smith, M., Deacon, P., 1996. Vestibulospinal, reticulospinal and descending propriospinal nerve fibres in man. Brain 119 (Pt 6), 1809–1833.

Soria, G., De Notaris, M., Tudela, R., Blasco, G., Puig, J., Planas, A.M., et al., 2011. Improved assessment of ex vivo brainstem neuroanatomy with high-resolution MRI and DTI at 7 Tesla. Anat. Rec. 294, 1035–1044.

Takano, M., Komaki, Y., Hikishima, K., Konomi, T., Fujiyoshi, K., Tsuji, O., et al., 2013. In vivo tracing of neural tracts in tiptoe walking Yoshimura mice by diffusion tensor tractography. Spine (38), E66–E72.

Thomas, C., Ye, F.Q., Irfanoglu, M.O., Modi, P., Saleem, K.S., Leopold, D.A., et al., 2014. Anatomical accuracy of brain connections derived from diffusion MRI tractography is inherently limited. Proc. Natl. Acad. Sci. U. S. A. 111, 16574–16579.

Yeh, F.C., Wedeen, V.J., Tseng, W.Y., 2010. Generalized q-sampling imaging. IEEE Trans. Med. Imaging 29, 1626–1635.

Zhao, M., Shi, B., Chen, T., Zhang, Y., Geng, T., Qiao, L., et al., 2017. Axial MR diffusion tensor imaging and tractography in clinical diagnosed and pathology confirmed cervical spinal cord astrocytoma. J. Neurol. Sci. 375, 43–51.